NASA/CR—2005-213561 AIAA–2005–1243

Validation Results for LEWICE 3.0

William B. Wright
QSS Group, Inc., Cleveland, Ohio

March 2005

The NASA STI Program Office . . . in Profile

Since its founding, NASA has been dedicated to the advancement of aeronautics and space science. The NASA Scientific and Technical Information (STI) Program Office plays a key part in helping NASA maintain this important role.

The NASA STI Program Office is operated by Langley Research Center, the Lead Center for NASA's scientific and technical information. The NASA STI Program Office provides access to the NASA STI Database, the largest collection of aeronautical and space science STI in the world. The Program Office is also NASA's institutional mechanism for disseminating the results of its research and development activities. These results are published by NASA in the NASA STI Report Series, which includes the following report types:

- TECHNICAL PUBLICATION. Reports of completed research or a major significant phase of research that present the results of NASA programs and include extensive data or theoretical analysis. Includes compilations of significant scientific and technical data and information deemed to be of continuing reference value. NASA's counterpart of peer-reviewed formal professional papers but has less stringent limitations on manuscript length and extent of graphic presentations.

- TECHNICAL MEMORANDUM. Scientific and technical findings that are preliminary or of specialized interest, e.g., quick release reports, working papers, and bibliographies that contain minimal annotation. Does not contain extensive analysis.

- CONTRACTOR REPORT. Scientific and technical findings by NASA-sponsored contractors and grantees.

- CONFERENCE PUBLICATION. Collected papers from scientific and technical conferences, symposia, seminars, or other meetings sponsored or cosponsored by NASA.

- SPECIAL PUBLICATION. Scientific, technical, or historical information from NASA programs, projects, and missions, often concerned with subjects having substantial public interest.

- TECHNICAL TRANSLATION. English-language translations of foreign scientific and technical material pertinent to NASA's mission.

Specialized services that complement the STI Program Office's diverse offerings include creating custom thesauri, building customized databases, organizing and publishing research results . . . even providing videos.

For more information about the NASA STI Program Office, see the following:

- Access the NASA STI Program Home Page at ***http://www.sti.nasa.gov***

- E-mail your question via the Internet to help@sti.nasa.gov

- Fax your question to the NASA Access Help Desk at 301–621–0134

- Telephone the NASA Access Help Desk at 301–621–0390

- Write to:
  NASA Access Help Desk
  NASA Center for AeroSpace Information
  7121 Standard Drive
  Hanover, MD 21076

NASA/CR—2005-213561 AIAA–2005–1243

Validation Results for LEWICE 3.0

William B. Wright
QSS Group, Inc., Cleveland, Ohio

Prepared for the
43rd Aerospace Sciences Meeting and Exhibit
sponsored by the American Institute of Aeronautics and Astronautics
Reno, Nevada, January 10–13, 2005

Prepared under Grant NAG3–00145

National Aeronautics and
Space Administration

Glenn Research Center

March 2005

Acknowledgments

The author would like to acknowledge Colin Bidwell, Mark Potapczuk, and Dean Miller from the NASA Glenn Icing Branch as well as Paul Tsao and David Anderson from the Ohio Aerospace Institute for their insight and experience with SLD issues. The author would also like to acknowledge Colin Bidwell and Mike Papadakis for insights into the experimental database that they had collected. The author would also like to acknowledge the continued financial support from NASA Glenn Research for this research.

Available from

NASA Center for Aerospace Information
7121 Standard Drive
Hanover, MD 21076

National Technical Information Service
5285 Port Royal Road
Springfield, VA 22100

Available electronically at http://gltrs.grc.nasa.gov

Validation Results for LEWICE 3.0

William B. Wright
QSS Group, Inc.
Cleveland, Ohio 44135

I. Abstract

A research project is underway at NASA Glenn to produce computer software that can accurately predict ice growth under any meteorological conditions for any aircraft surface. This report will present results from version 3.0 of this software, which is called LEWICE. This version differs from previous releases in that it incorporates additional thermal analysis capabilities, a pneumatic boot model, interfaces to computational fluid dynamics (CFD) flow solvers and has an empirical model for the supercooled large droplet (SLD) regime. An extensive comparison of the results in a quantifiable manner against the database of ice shapes and collection efficiency that have been generated in the NASA Glenn Icing Research Tunnel (IRT) has also been performed. The complete set of data used for this comparison will eventually be available in a contractor report. This paper will show the differences in collection efficiency between LEWICE 3.0 and experimental data. Due to the large amount of validation data available, a separate report is planned for ice shape comparison. This report will first describe the LEWICE 3.0 model for water collection. A semi-empirical approach was used to incorporate first order physical effects of large droplet phenomena into icing software. Comparisons are then made to every single element two-dimensional case in the water collection database. Each condition was run using the following five assumptions: 1) potential flow, no splashing; 2) potential flow, no splashing with 21 bin drop size distributions and a lift correction (angle of attack adjustment); 3) potential flow, with splashing; 4) Navier-Stokes, no splashing; 5) Navier-Stokes, with splashing. Quantitative comparisons are shown for impingement limit, maximum water catch and total collection efficiency. The results show that the predicted results are within the accuracy limits of the experimental data for the majority of cases.

II. Nomenclature

a	correlation parameter for curve-fit (dimensionless)
A_p	cross-sectional area of particle (m^2)
c	chord (m)
D	drag force ($kg*m/s^2$)
D_{le}	Airfoil leading edge diameter (m)
d	particle diameter (m)
E	total water collection efficiency (dimensionless)
f	drop frequency (Hz)
g	gravitational constant = 9.8 m/s^2
h	film thickness (m)
L	lifting force ($kg*m/s^2$)
LWC	liquid water content (g/m^3)
m	particle mass (kg)
$\dot{m}$	water mass flux (kg/m^2 s)
n	correlation parameter for curve-fit (dimensionless)
s	surface wrap distance (m)
s_l	lower impingement limit by wrap distance (m)
s_{l10}	lower limit by wrap distance where β = 10% (m)
s_u	upper impingement limit by wrap distance (m)
s_{u10}	upper limit by wrap distance where β = 10% (m)

t	Time (s)
V	relative droplet velocity (m/s)
V_x	x-component of velocity (m/s)
V_y	y-component of velocity (m/s)
x	horizontal direction (m)
x_l	lower impingement limit by x-location (m)
x_{l10}	lower limit by x-location where β = 10% (m)
x_u	upper impingement limit by x-location (m)
x_{u10}	upper limit by x-location where β = 10% (m)
x_p	x-location of water particle (m)
$\dot{x}$	first derivative of x-location of water particle with respect to time (x-component of particle velocity) (m/s)
$\ddot{x}$	second derivative of x-location of water particle with respect to time (x-component of particle acceleration) (m/s^2)
y	vertical direction (m)
y_0	y-value of the starting locations of collection efficiency trajectories (m)
y_p	y-location of water particle (m)
$\dot{y}$	first derivative of y-location of water particle with respect to time (y-component of particle velocity) (m/s)
$\ddot{y}$	second derivative of y-location of water particle with respect to time (y-component of particle acceleration) (m/s^2)

A. Dimensionless Numbers

c_l	coefficient of lift $= \dfrac{L}{A_p \rho_a V^2/2}$
c_d	coefficient of drag $= \dfrac{D}{A_p \rho_a V^2/2}$
f*	dimensionless drop frequency $= f\dfrac{d}{V}$
K	Mundo splashing parameter $= Oh\,\mathrm{Re}^{5/4}$
K_L	LEWICE splashing parameter $= K^{0.859}\left(\dfrac{\rho_w}{LWC}\right)^{0.125}$
K_{Ln}	normal component of LEWICE splashing parameter $= \dfrac{K_L}{(\sin\theta_i)^{1.25}}$
K_o	modified inertia parameter $= 0.125 + \left(\dfrac{\rho_w d^2 V}{18\mu_w D} - 0.125\right)\left(\dfrac{1}{0.8388 + 0.001483\mathrm{Re} + 0.1847\sqrt{\mathrm{Re}}}\right)$
La	Laplace number $= \dfrac{\rho_w \sigma d_o}{\mu^2}$
Oh	Ohnesorge number $= \dfrac{\mu}{\sqrt{\rho\sigma d}}$
Re	Reynolds number $= \dfrac{\rho V d}{\mu}$
We	Weber number $= \dfrac{\rho V^2 d}{\sigma}$

B. Greek Letters

α	angle of attack (degrees)
β	collection efficiency (dimensionless)
γ	angle difference between particle velocity vector and airflow velocity vector (radians)
δ	film thickness (dimensionless = h/d)

μ viscosity (kg/m*s)
ν kinematic viscosity of air (m^2/s)
ρ density (kg/m^3)
σ surface tension (kg/s^2)
θ impact angle (degrees)

C. Subscripts

a air
b bouncing
c critical
le leading edge
max maximum value
n normal direction
o initial value
p particle
s splashed (or secondary) drop value
t tangential direction
term terminal
w water
x x-dependent
y y-dependent
∞ free-stream property

III. Introduction

In 1994, an ATR-72 crashed in Roselawn, IN[1]. It has been speculated that accident occurred due to the accumulation of ice aft of the deicing boots. Ice formed aft of the boots due to impingement of drops greater than 40 μm. Since then, several experimental efforts have been made to document supercooled large droplet (SLD) ice shapes and to investigate the underlying physics[2-7]. Based on this experimental work, an empirical model was developed to account for large droplet effects in LEWICE. This model was reported on last year[8].

This report will address the validation of that model against a database of water collection efficiency data that has been generated over the course of several years[9-11]. This validation effort mirrors a similar effort undertaken previously for the validation of LEWICE for ice shapes[12]. That report quantified the ice accretion prediction capabilities of the LEWICE 2.0 software. Several ice geometry features were proposed for comparing ice shapes in a quantitative manner. The resulting analysis showed that LEWICE 2.0 compared well to the available experimental data. The purpose of this report is to present a similar process for comparing water collection efficiencies.

The report is divided into four sections. The first section will provide a description of the LEWICE software and the Naviér-Stokes flow solver WIND[13] that was used for this effort. The second section will provide a description of the LEWICE collection efficiency model with emphasis on breakup and impact physics. It will also describe the modified equations including analysis and observations from tests performed in the NASA icing research tunnel (IRT). The third section will describe the experimental data and the parameters used for quantifying the comparisons. The last section will provide validation results along with a statistical comparison of those parameters with the available experimental data.

IV. Computational Tools

A. LEWICE

The computer program, LEWICE, embodies an analytical ice accretion model that evaluates the thermodynamics of the freezing process that occur when supercooled droplets impinge on a body. The atmospheric parameters of temperature, pressure, and velocity, and the meteorological parameters of liquid water content (LWC), droplet diameter, and relative humidity are specified and used to determine the shape of the ice accretion. The surface of the clean (un-iced) geometry is defined by segments joining a set of discrete body coordinates. The software consists of four major modules. They are 1) the flow field calculation, 2) the particle trajectory and impingement calculation, 3) the thermodynamic and ice growth calculation, and 4) the modification of the current geometry by addition of the ice growth.

LEWICE applies a time-stepping procedure to "grow" the ice accretion. Initially, the flow field and droplet impingement characteristics are determined for the clean geometry. The ice growth rate on each segment defining the surface is then determined by applying the thermodynamic model. When a time increment is specified, this growth rate can be transformed into an ice thickness and the body coordinates are adjusted to account for the accreted ice. This procedure is repeated, beginning with the calculation of the flow field about the iced geometry, then continued until the desired icing time has been reached. The results shown in this report are from version 3.0 of LEWICE[14].

B. WIND

WIND is a structured, multi-zone, compressible flow solver with flexible chemistry and turbulence models. Zonal interfaces may be abutting or overlapped, allowing the flexibility to treat complex systems moving relative to one another. WIND is a computational platform that may be used to numerically solve various sets of equations governing physical phenomena. Currently, the software supports the solution of the three-dimensional Euler and Naviér-Stokes equations of fluid mechanics, along with supporting equation sets governing turbulent and chemically reacting flows.

WIND is a product of the NPARC Alliance, a partnership between the NASA Glenn Research Center (GRC) and the Arnold Engineering Development Center (AEDC) dedicated to the establishment of a national, applications-oriented flow simulation capability. The Boeing Company has also been closely associated with the Alliance since its inception, and represents the interests of the NPARC User's Association.

C. ICEG2D

ICEG2D[15] is an automated grid generation program and scripting interface. The grid generation capability contains algorithms for producing single block “C” grids. The scripting portion of the software provides an interface between LEWICE and WIND. Flow field information from WIND is processed through the WIND utility GMAN and formatted for use in LEWICE. LEWICE then sends the completed ice shape back to ICEG2D for the next icing time step.

V. Collection Efficiency Physics

Collection efficiencies are calculated in LEWICE through the use of a particle trajectory analysis. Droplets are released from a point in the freestream flow and tracked through the flow field using the following equations:

$$m\ddot{x}_p = -D\cos\gamma - L\sin\gamma \qquad\qquad m\ddot{y}_p = -D\sin\gamma + L\cos\gamma - mg$$

where $$\gamma = a\tan\frac{\dot{y}_p - V_y}{\dot{x}_p - V_x}, \qquad D = c_d\frac{\rho_a V^2}{2}A_p, \qquad L = c_l\frac{\rho_a V^2}{2}A_p, \qquad V = \sqrt{(\dot{x}_p - V_x)^2 + (\dot{y}_p - V_y)^2}$$

The initial release point in the x-direction is determined by finding an x-location where all of the velocities in a vertical sweep are within 0.1% of the freestream value. The initial release point in the y-direction is determined from the angle of attack. The initial velocity is assumed to be the terminal droplet velocity, which is given by

$$c_d\,\mathrm{Re}_{term}^2 = \frac{4gd\,(\rho_w - \rho_a)}{3\nu_a^2\rho_a} \qquad \text{where} \qquad \mathrm{Re}_{term} = \frac{V_{term}d}{\nu_a}$$

Each droplet is then tracked until it either hits the airfoil or reaches the trailing edge. After the first trajectory ends, the next particle is released from a higher or lower starting point in an attempt to hit the surface. This process is continued until there exists at least one drop that passes above the airfoil and one that passes below.

Impingement limits are then found using a standard bisection search algorithm. Using the coarse limits found in the prior step, LEWICE starts a drop halfway between these limits. Based upon the end result of that trajectory, the next drop is released halfway between the current starting point and the starting point of either the upper or lower coarse limit. The coarse limit is then refined based upon the trajectory results. This process is repeated until the starting point of a drop that hits the airfoil and the starting location of a drop that misses the airfoil is within 10^{-5}. The bisection is then repeated to find the second impingement limit.

Collection efficiency is then determined by sending a user-determined number of trajectories uniformly spaced between the impingement limit starting locations. The starting and ending locations of these trajectories is stored. Collection efficiency is then calculated by the following definition:

$$\beta \equiv \frac{dy_o}{ds}$$

A. Literature review

This section will present various assumptions used in the collection efficiency calculation in LEWICE. While other surface physics such as evaporation, rivulet flow and film dynamics are important to the water impact, much of this review centers on trajectory and splashing phenomena. The review will focus on effects for larger droplets. A large drop in this context applies to any drop size larger than 40μm, the current upper limit in the FAA certification envelope. LEWICE uses the following assumptions in the trajectory equations:

solid particles
initially spherical particles
drops break up completely
particles do not rotate
Saffman lift is modeled
particles have no moment
drag for a stationary water particle applies
no transient effects of drag
evaporation of the drop is negligible
turbulence effects are neglected
gravity is considered
drops do not interact with each other
slip flow around drop is empirically modeled
drops that strike the airfoil impinge unless splashing criteria are met
splashed drops are monodispersed
splashed drop size, velocity and angle are empirically based

Droplet motion and impact has a wide variety of applications and has been studied extensively in several research areas. Much of the early work was summarized by Clift, Grace and Weber[16] and also by Tavlarides et. al.[17]. A summary of more recent research was performed by Michaelides[18]. A previous report provided more detail of the pertinent large droplet physics[8]. While many of these physical effects can be studied, this report will focus on those that have the most impact on collection efficiency.

1. Drop Breakup

If a large drop moves at a high enough velocity, it can breakup due to shear. Breakup occurs when the drop passes a critical Weber number. Values for this critical Weber number vary widely in the literature.

The Weber number is given by:

$$We_p = \frac{\rho_a V^2 d}{\sigma}$$

For water drops falling at their terminal velocity, the critical Weber number (based on air density) is approximately 10. For water drops accelerated by a shock wave, a value of 6.5 is given. Krzeczkowski[19] and Hsiang[20] each measured droplet breakup for shear induced flows and reported values ranging from 10 to 20. Ibrahim et. al.[21] provided a more detailed analysis of the droplet deformation and breakup using a Taylor analogy model. The Weber number of each trajectory was output from LEWICE for the case described above to investigate this effect. A contour plot of Weber number is shown in Figure 1 and shows that the Weber number clearly indicates that drop breakup occurs for this drop size.

Figure 1: Weber Number on a 1000 micron drop

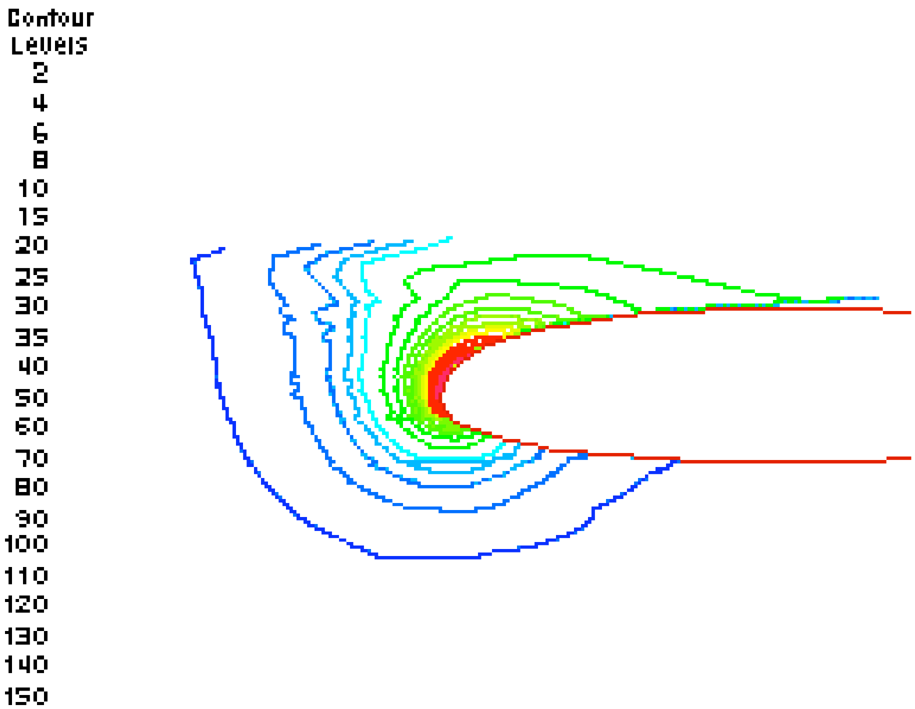

The case for a 1000μm drop clearly shows that according to the Weber number criteria, drops will breakup before reaching the airfoil. The breakup criteria is reached by the first green line in the figure above. At this point, it is unclear how this breakup affects the collection efficiency. The smaller drops produced by the breakup will tend to be deflected more. By the time the drops reach critical Weber number values, they are only 0.1 chord from the leading edge even in this extreme example. As most of the particle deflection occurs within this region and since drops tend to break up into much smaller drops, it seems feasible that there is some mass loss that can be attributed to this factor.

An empirical relationship found in Hsiang and Faeth[20] was added to LEWICE in order to estimate the reduction of collection efficiency due to breakup. In their model, droplets will start to break up when the critical Weber number is greater than 13. This Weber number is based on the air density as defined earlier in this report. Since droplet breakup occurs rapidly compared to the trajectory time step, breakup is considered to be instantaneous. Dai and Faeth[22] produced some excellent photographs of the breakup process using pulsed shadowgraphy and holography.

Secondary particle size is given by the following equation:

$$d_s = 6.2\left(\frac{\rho_w}{\rho_a}\right)^{1/4} \mathrm{Re}_w^{-1/2}\, d_o \qquad \text{where} \qquad \mathrm{Re}_w = \frac{\rho_w V d}{\mu_w}$$

This correlation can be applied to an Eulerian system as well as the Lagrangian tracking system used by LEWICE. However, it would be necessary in a Eulerian system to solve coupled sets of equations for each drop size generated. In the Lagrangian system, the smaller drop size is simply tracked from the breakup location. An empirical relationship was chosen to assess the importance of breakup to the collection efficiency. If breakup is not important then there is no need to implement the more complicated droplet deformation and breakup (DDB) model described by Ibrahim[21].

2. Drop Splashing

The literature search performed for this report confirms that the primary assumption used by LEWICE 2.0 that was invalidated for SLD was the assumption that all drops that strike the surface impinge, thus neglecting splashing and/or bouncing of drops. One of the earliest detailed experimental studies was performed by Stow and Hadfield[23] who reported on the impact of water drops on a dry surface. Macklin and Metaxas[24] reported a similar study that also used ethanol and glycerol to study the effect of different fluid properties. Jayarante and Mason[25] looked at bouncing and splashing of raindrops impinging at various angles on dry surfaces and films. Wright[26] developed a theoretical splash model for raindrops for the purpose of modeling soil erosion.

Harlow and Shannon[27] solved the Naviér-Stokes equations for the impact of a single drop on a dry surface or film. A more recent work was performed by Yarin and Weiss[28, 29] who proposed a splashing model as a type of kinematic discontinuity. Other works include Rein[30] who provides a review of several papers, including phenomena such as bouncing along with splashing and coalescence and Chandra and Avedisian[31] who documented photographically the droplet structure during the deformation process.

Computationally, a detailed physical model of droplet splashing would require solving the Naviér-Stokes equations for each droplet impact using a Volume of Fluid (VOF) model such as that described by Hirt[32]. Examples of this type of calculation were reported by Trapeaga and Szekely[33] as well as Tan and Papadakis[2]. Current computational capabilities usually limit this approach to single drop calculations. In a typical icing encounter, thousands of droplet impacts are recorded per second, making this type of analysis prohibitively expensive. An empirical or semi-empirical approach is therefore necessary.

A recent experimental study by Mundo, Sommerfeld and Tropea[34-6] examined droplet-wall collisions and correlates splashing in terms of Reynolds number and Ohnesorge number

$$Oh = \frac{\sqrt{We}}{\mathrm{Re}} = \frac{\mu}{\sqrt{\rho\sigma d}}$$

The Reynolds and Ohnesorge numbers are based on the liquid (water) properties and the component of the impact velocity normal to the surface. Based on the results of their experiment, splashing occurs if the factor $K=Oh*Re^{1.25}$ is greater than 57.7. A plot of this parameter for drop sizes of 20 and 200 microns is shown in Figure 2.

Figure 2: K-factor for droplet splash

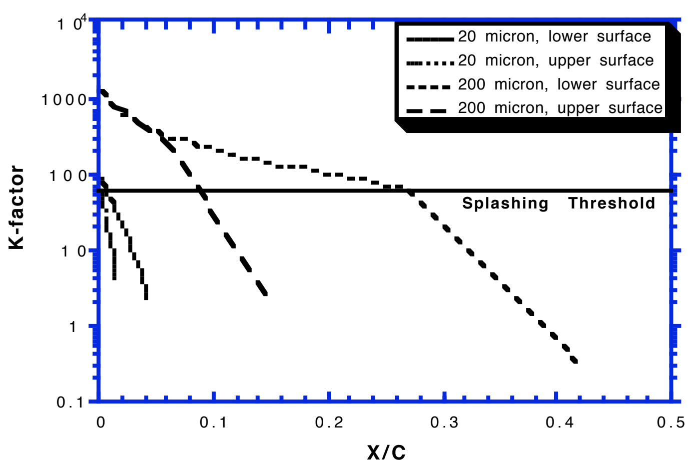

A small amount of droplet splash near the leading edge is seen in Fig. 2 even for the 20 micron drop results, shown by the first two lines. This demonstrates that splashing will occur at much lower drop sizes than droplet break up. This figure also shows that droplet splashing is a significant factor in the large drop regime.

The Mundo papers also provide a characterization of the size, velocity and direction of the splashed particles. Their later references provide an empirical splashing model that can be used in Lagrangian tracking schemes. The empirical formulas calculate splashed drop size, splash velocity, splash angle and deposited mass as functions of the incoming parameters. The Mundo expressions are given below.

$$K = \left(\frac{\rho_w^3 d^3 V_n^5}{\sigma^2 \mu_w}\right)^{1/4} \geq 57.7 \text{ for splash} \quad ; \quad \frac{d_s}{d_o} = 8.72 e^{-0.0281K};\ 0.05 \leq \frac{d_s}{d_o} \leq 1$$

$$n_s = 1.676 * 10^{-5} K^{2.539};\ n_s \leq 1000 \quad ; \quad \frac{m_s}{m_o} = n_s \left(\frac{d_s}{d_o}\right)^3$$

$$\frac{V_{t,s}}{V_{t,o}} = 1.337 - 1.318 \frac{d_s}{d_o} + 2.339 \left(\frac{d_s}{d_o}\right)^2 \quad ; \quad \frac{V_{n,s}}{V_{n.o}} = -0.249 - 2.959 \frac{d_s}{d_o} + 7.794 \left(\frac{d_s}{d_o}\right)^2$$

Some observations can be derived from these expressions. First, for K < 77, drops bounce (size out = size in). At the splashing onset (K=57.7), roughly half will bounce, since half the mass is lost and the size of the drops has not changed. At K = 77, all of the drops will bounce, as the outbound size has not changed and the mass loss is 100%. According to this model, the breakup of a drop into smaller particles doesn't really occur until K > 77. Splash mass is 0.15% at the upper K limit and shows asymptotic behavior. Finally, these correlations are only valid up to a drop size of 150μm and a drop speed of 18 m/s. This range is much lower than that needed for icing analysis.

However, there are additional problems with this approach. If it is assumed that the splashing measured by Mundo scales into the icing regime (higher velocity and initial drop size), then maximum mass loss (K = 77) would be greatest in the Appendix C regime, not SLD. Additionally, the correlations given above do not make physical sense. For example, their report gives 1000 as the maximum number of drops that can be generated from a single splash. However, the correlation gives only nine drops generated at K = 180, the upper limit of his data. Mundo also gives droplet velocity correlations that do not conserve momentum at the lower range of his K-values.

Based on these discrepancies, additional reports were sought to determine correlations more suited for use in icing. Several authors provided empirical models for the splashing threshold or for splashed drop size. However, a complete model including splashed mass loss and splashed velocity was sought so that it could be implemented into LEWICE. The following section provides a summary of the current splashing model.

3. Summary of LEWICE Splashing Model

The parameters needed for an empirical splashing model are the splashing threshold, the splashed drop size (or drop size distribution), the splashed velocity (or a distribution of splash velocities), the splash angle (or a distribution of splash angles) and the amount of splashed mass. The number of splashed particles is needed only if all splashed particles are to be tracked. The models presented in the literature typically provide these variables as a ratio to the incoming parameters.

Many of the splashing models include the effects of droplet frequency, f, and the dimensionless film thickness δ. As stated earlier, splashed droplets are likely to interact with incoming drops. Since this physical effect occurred in the experiments reviewed, it was assumed unnecessary to otherwise account for droplet-droplet interactions. Droplet frequency can be calculated from the liquid water content by assuming that particles are uniformly distributed in the freestream. The drop frequency is given by the following equation:

$$f = \frac{3}{2}\frac{V}{d}\left(\frac{LWC}{\rho_w}\right)^{1/3}$$

The correlations implemented into LEWICE calculate frequency from the MVD and the overall LWC. If necessary, it could also be calculated from the individual droplet spectrum. Film thickness was estimated from a correlation provided by Feo[37]:

$$\delta = 3.76 \left(\frac{D_{le}}{d}\right)^{5/4} \left(\frac{LWC}{\rho_w}\right)^{1/2} We_{le}^{-1/8} \qquad \text{where} \qquad \delta = \frac{h}{d}$$

The droplet experiments that the LEWICE correlation is based on (Mundo[34-6], Trujillo[38] and others mentioned) were developed using similar experimental techniques and therefore had similar ranges of applicability. The upper limit on drop size and velocity were 340μm and 30 m/s respectively. Droplet frequency and film thicknesses were in the range expected for icing encounters except at the lower range. Splash data exists for dry surfaces ($\delta = 0$) and for film thicknesses of $0.3 < \delta < 3$. The applicability of these models to very thin films is unknown. Similarly, droplet frequencies are lower in the SLD range due to the lower water contents as well as the higher drop sizes. However, the correlations are well behaved in these limits and tend toward limiting values.

Trujillo et. al.[38] used Mundo's drop size expression but used different forms for the other variables. Their correlation can be expressed by:

$$\frac{V_{t,s}}{V_{t,o}} = 0.85 + 0.0025\theta_o \quad ; \quad \frac{V_{n,s}}{V_{n,o}} = 0.12 + 0.002\theta_o$$

$$\frac{m_s}{m_o} = 0.2\left[1 - \exp\left(K^{1/2} f^{*^{-3/8}} - K_c^{1/2} f_c^{*^{-3/8}}\right)\right] \quad ; \quad n_s = \frac{1}{22}\left[0.0437\left(K\left(\frac{V_{x,o}}{V_{y,o}}\right)^2 - K_c\right) - 44.92\right]$$

LEWICE uses a modified version of the Trujillo expressions. The exact equations are given by:

Splashing threshold: $K_{L,n} > 17$ where $K_{L,n} = \sqrt{K} f^{*^{-3/8}}$

$$\frac{d_s}{d_o} = 8.72e^{-0.0281K},\ 0.05 \le \frac{d_s}{d_o} \le 1 \quad ; \quad \frac{m_s}{m_o} = 0.2\left[1 - \exp\left(0.85 * \left(K_{L,n} - 17\right)\right)\right]$$

$$\frac{V_{t,s}}{V_{t,o}} = 1.075 - 0.0025\theta_o \quad ; \quad \frac{V_{n,s}}{V_{n,o}} = 0.3 - 0.002\theta_o$$

In addition, a bouncing model was incorporated into LEWICE. The addition of a droplet bouncing expression was justified by noting that the splashing expressions given above will have their largest effect near the leading edge while the experimental data for collection efficiency demonstrated a large effect near the impingement limits. It is hypothesized by the author that the additional mass loss near the impingement limits would be due to bouncing of the drops. Bouncing phenomena are common occurrences with droplet impacts. There have been other bouncing regimes in the $5 < We < 10$ range noted in the literature. This lower Weber number range was not modeled in LEWICE due to the narrow band in which it occurs. Some of the reports previously mentioned also denote alternating regimes of bouncing and splashing. Since droplet impact phenomena at the high velocities encountered in aircraft icing have not previously been studied in the literature, it is reasonable to assume that additional phenomena could be present at these velocities. The current bouncing model was based upon the experimental collection efficiency results[9-11] for the MS-317 model at 0° and 8° angle of attack and a drop size of 92 µm. Droplet bouncing was chosen instead of splashing due to the occurrence of alternating regions of bouncing and splashing noted at lower velocities. **The bouncing model is described by the following equations:**

Bouncing threshold: $K_L > 300$ and $\theta_o < 30°$ where $K_L = K_{L,n} / (\sin \theta_o)^{1.25}$

$$\frac{m_b}{m_o} = \frac{K_L - 260}{200}$$

with the constraints that the mass loss due to bouncing must be greater than or equal to the splashing mass loss and less than or equal to 1.

The bouncing mass loss is used instead of (not in addition to) the splashing mass loss if the bouncing threshold constraint is met. In this model, bouncing is proportional to the total impact parameter, not simply the normal component as was the case with the splashing model. Bouncing would also not occur except when the impact angle was less than 30°. These assumptions were justified by hypothesizing that bouncing occurred due to the high momentum of the particles and that drops might glance off the airfoil at low impact angles. The bouncing magnitude was empirically determined by the two cases mentioned above.

By knowing the bouncing and splashing parameters, a feature was added to LEWICE to track the trajectories of the splashed particles and the trajectories of particles after breakup. This process was described in a recent report by Rutkowski, et. al.[7]. Mass losses due to splashing and subsequent reimpingement are also calculated. Since it is necessary to extrapolate from the experimental data for icing encounters, care must be taken, especially in high velocity impacts. The equations provided above indicate that droplet velocity (which is related to airspeed) is at least as important to the splashing process as drop size. Care should be taken when running cases at velocities higher than those in the database (175 mph) from which this model was derived. The next section will describe the experimental data in more detail.

VI. Experimental Data

The experimental data used for this comparison was taken from several tests performed in the IRT[9-11]. The tests were performed by personnel from Wichita State University, NASA and Boeing using a specialized spray system designed for short duration sprays. The water spray contains a known concentration of blue dye and the models are covered with a heavy weight blotter paper. The amount of dye was then measured via reflectance spectroscopy using a CCD camera. Collection efficiencies were determined on 11 different clean airfoils and 7 different iced airfoils. Drop size distributions from MVDs of 11 μm to 236 μm and angle of attack were varied from 0° to 8°. Table 1 contains a list of the conditions for this database. For brevity, similar conditions have been listed together. As an example, the NACA64A008 database consists of six cases: at 0° and 6° angles of attack, collection efficiencies were obtained for each of the three drop sizes listed. There are 117 distinct cases in the database and the airspeed for all cases was 175 mph.

Table 1: Database Conditions

Airfoil	AOA	MVD (micron)	Chord (ft)	V (mph)
NACA 64A008 Finite Swept Tail	0, 6	11.5, 21, 92	3.14	175
NACA 65(2)-415 Airfoil	0	11.5, 21, 79, 92, 137, 168	3.04	175
NACA 65(2)-415 Airfoil	4	11.5, 21, 79, 137, 168	3.04	175
NACA 65(2)-415 Airfoil	8	11.5, 21, 92	3.04	175
GLC-305 Airfoil	1.5	11.5, 21, 79, 92, 137, 168	3.00	175
GLC-305 Airfoil	6	11.5, 21, 92	3.00	175
Full-scale Business Jet Tail Section	1	11, 21, 94	2.68	175
Full-scale Business Jet Tail Section	6	21	2.68	175
Commercial Jet Transport Tail Section	0,4	11.5, 21, 92	3.00	175
MS(1)-317 Airfoil	0	11.5, 21, 79, 92, 137, 168	3.00	175
MS(1)-317 Airfoil	8	11.5, 21, 92	3.00	175
NACA 23012 Airfoil	2.5	20, 52, 111, 154, 236	3.00	175
NACA 23012 & 5-min Glaze Ice Shape	2.5	20, 52, 111, 154, 236	3.00	175
NACA 23012 & 10-min Glaze Ice Shape	2.5	20, 52, 111, 154, 236	3.03	175
NACA 23012 & 15-min Glaze Ice Shape	2.5	20, 52, 111, 154, 236	3.04	175
NACA 23012 & 22.5-min Glaze Ice Shape	2.5	20, 52, 111, 154, 236	3.05	175
NACA 23012 & 45-min Glaze Ice Shape	2.5	20, 52, 111, 154, 236	3.19	175
Twin Otter Tail Section	0,4	11, 21, 79, 137, 168	4.75	175
Twin Otter & 22.5-min Glaze Ice Shape	0	11, 21, 79, 168	4.83	175
Twin Otter & 45-min Glaze Ice Shape	0	11, 21, 79, 168	4.97	175
36" NLF(1)-414 Airfoil	0,8	11, 21, 94	3.00	176
48" NLF(1)-414 Airfoil with Flap	0,4,8	11, 21, 94	4.00	175
48" NLF(1)-414 Airfoil with Flap Deflected	0	11, 21, 94	4.00	175
MD 3-Element High Lift System	0,4	11.5, 21, 92	3.00	175

The database consists of a wide variety of airfoils that were selected to provide a broad range of airfoil types for validation purposes. The MS-317 airfoil shown in Fig. 3 was chosen as representative of modern medium speed airfoils. The GLC-305 airfoil shown in Fig. 4 was chosen as representative of a general aviation business jet wing and the NACA 64A008 shown in Fig. 5 was chosen as representative of a tail section. The NLF(1)-414 and NACA 65(2)-415 shown in Figs. 6 & 7 were chosen as examples of general aviation wings. The commercial jet tail, the business jet tail and the Twin Otter tail sections shown in shown in Figs. 8-10 were chosen as representative tail sections. The NACA 23012 airfoil shown in Fig. 11 was chosen as representative of a small commuter class airfoil. The conditions for the ice shapes shown in Figs. 12 & 13 were chosen from within the Appendix C envelope as a severe glaze condition that might be used for FAA compliance as a 45 minute hold unprotected surface case. The ice shapes were produced using LEWICE 2.2.2 with the following conditions: MVD, 21 μm; LWC, 0.5 g/m^3; AOA, 2.5°; V, 152 kts, T, 22.5 °F. The drop size distributions were measured during the experiment and unless otherwise noted were modeled in LEWICE using 10-bin distributions. Tables 2 and 3 list the distributions used for this comparison. The estimated experimental repeatability for this data ranged from 10% to 30% for the older data sets. An uncertainty analysis presented in the reports on the experimental data showed that uncertainty in spray time, dye concentration, spray pressures, tunnel velocity and cloud unsteadiness due to turbulence accounted for a 14% variation in maximum collection efficiency values. In the following comparison with predicted results, the 14% value was used as representative of the experimental error for all parameters. Specific variability of individual parameters could not be defined[39].

Figure 3: MS-317 Airfoil

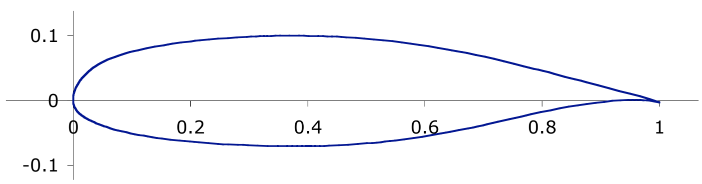

Figure 4: GLC-305 Airfoil

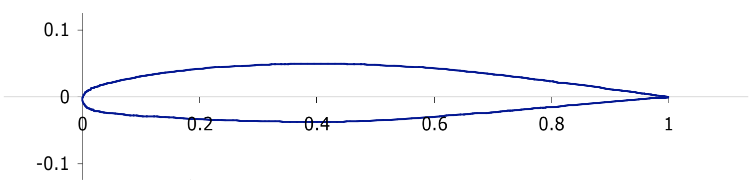

Figure 5: NACA 64A008 Airfoil

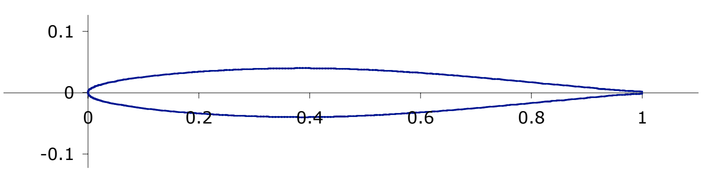

Figure 6: NLF(1)-414 Airfoil

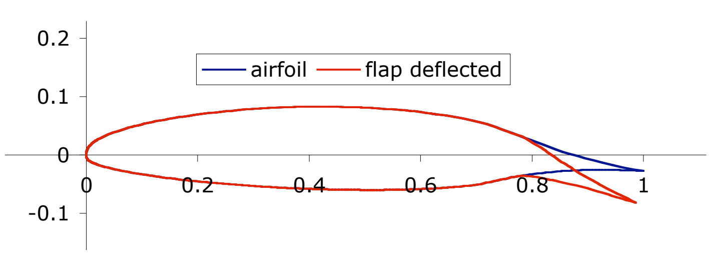

Figure 7: NACA 65(2)-415 Airfoil

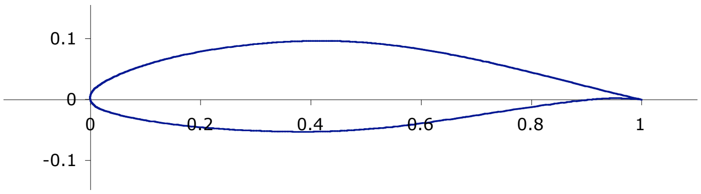

Figure 8: Business Jet Tail

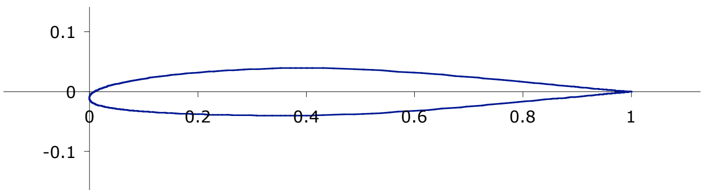

Figure 9: Commercial Jet Transport Tail

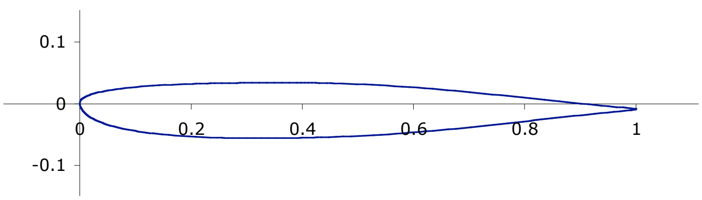

Figure 10: Twin Otter Tail

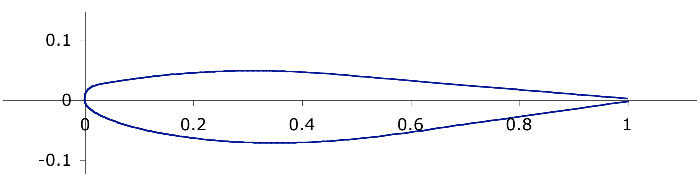

Figure 11: NACA 23012 Airfoil

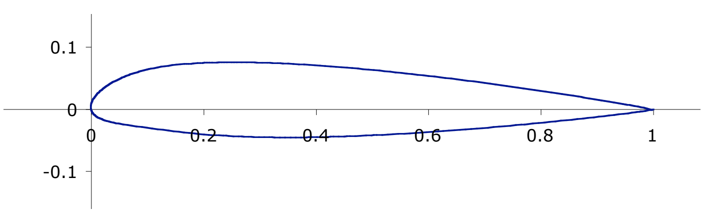

Figure 12: Ice Shapes on the Twin Otter Tail

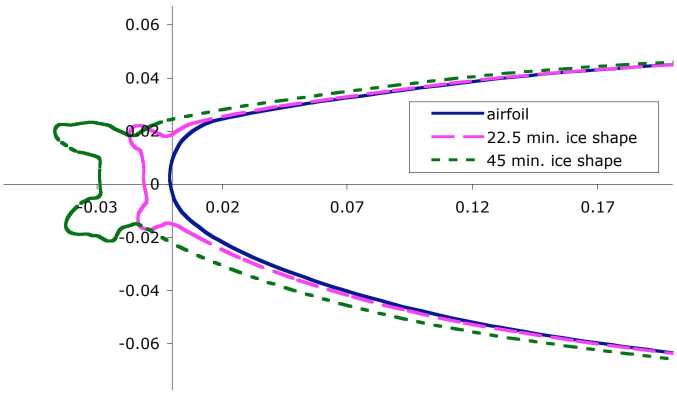

Figure 13: Ice Shapes on the NACA 23012 Airfoil

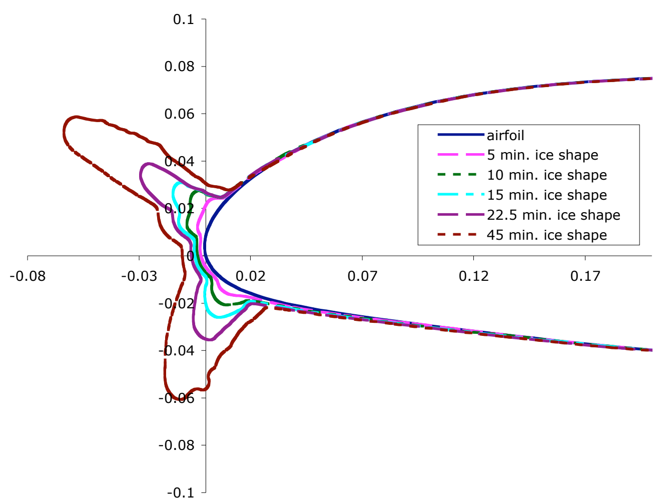

Table 2: LEWICE Drop Size Distributions

MVD = 11.5		MVD = 21		MVD = 52		MVD = 79		MVD = 92	
FLWC	DS	FLWC	DS	FLWC	DS	FLWC	DS	FLWC	DS
0.0245	3.5	0.1390	8.6	0.050	6.7	0.05	9.1	0.01	10.9
0.1449	6.5	0.0958	12.5	0.100	16.9	0.1	22.4	0.064	21.8
0.3327	9.5	0.0997	15.5	0.200	25.4	0.2	39.9	0.106	31.8
0.2170	12.5	0.1220	18.5	0.300	59.2	0.3	77.5	0.073	43.8
0.1389	15.5	0.1208	21.5	0.200	131.3	0.2	123.6	0.135	69.2
0.0955	18.5	0.1115	24.5	0.100	192.8	0.1	166.6	0.164	98.2
0.0362	21.5	0.0917	27.5	0.030	216.6	0.03	206.5	0.149	126.7
0.0089	24.5	0.0946	31.6	0.010	225.0	0.01	241.5	0.103	157.8
0.0011	27.5	0.0899	48.2	0.005	229.0	0.005	270.4	0.13	196.3
0.0002	30.5	0.0350	95.9	0.005	253.9	0.005	310.3	0.065	241.4

Table 3: LEWICE Drop Size Distributions

MVD = 105		MVD = 137		MVD = 151		MVD = 168		MVD = 236	
FLWC	DS	FLWC	DS	FLWC	DS	FLWC	DS	FLWC	DS
0.0102	10.9	0.05	13.3	0.060	21.7	0.05	15.1	0.0249	20.8
0.0640	21.8	0.10	41.8	0.061	33.1	0.1	52.5	0.0655	37.1
0.1057	31.8	0.20	81.4	0.063	48.5	0.2	102.3	0.0961	89.6
0.0735	43.8	0.30	138.2	0.154	85.9	0.3	172.1	0.1468	144.7
0.1353	69.2	0.20	206.8	0.192	128.0	0.2	264.4	0.1411	203.4
0.1639	98.2	0.10	285.3	0.183	172.4	0.1	395.6	0.0853	260.9
0.1495	126.7	0.03	382.6	0.146	215.7	0.03	530.9	0.0416	320.8
0.1030	157.8	0.01	471.5	0.086	265.0	0.01	624.5	0.0231	382.6
0.1295	196.3	0.00	534.1	0.032	324.0	0.005	705.4	0.2139	487.5
0.0654	241.4	0.00	693.9	0.023	414.0	0.005	1110.8	0.1617	675.1

VII. Results and Comparison Methodology

The comparison process for collection efficiency mimics the process used in a previous report[12] for comparing ice shapes. The following six parameters were chosen to represent the collection efficiency results: maximum collection efficiency (β_{max}), total collection efficiency (E) which is proportional to total water catch rate, upper & lower impingement limits (s_u and s_l) and the location on the upper & lower surface where collection efficiency reached 10% (s_{u10} and s_{l10}). These parameters are shown on a representative collection efficiency curve in Figure 14 below. The parameters are labeled on the figure for both the experimental and numerical results. The example shown contains collection efficiency for the MS317 airfoil at 0° AOA and 92 μm MVD. While this figure depicts the impingement distance based on wrap distance, the impingement limit comparisons were done using the x-distance from the leading edge. For the ice shape cases, x/c = 0 represents the leading edge of the clean airfoil geometry.

Figure 14: Sample Collection Efficiency Curve

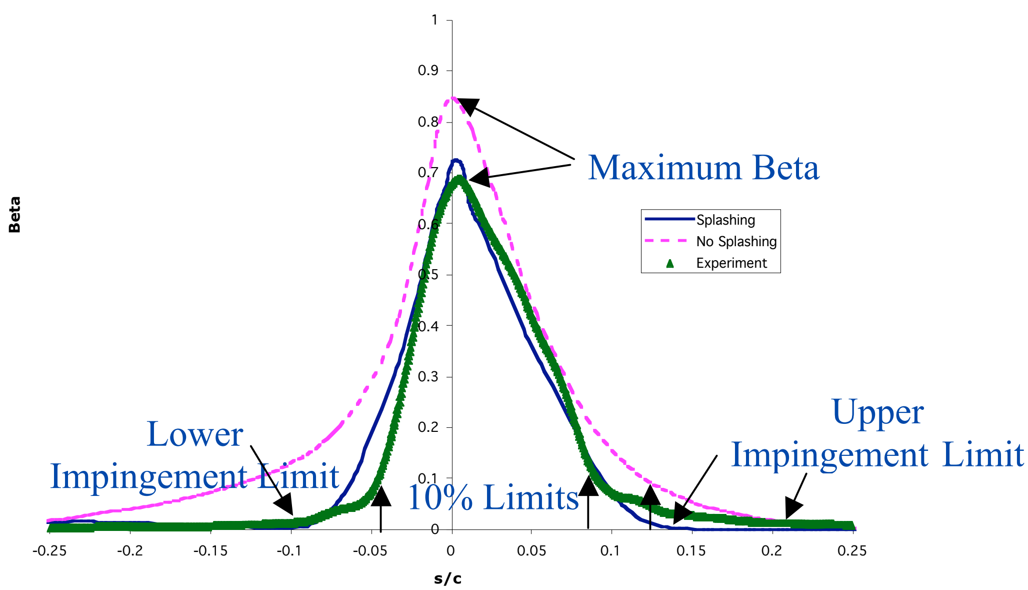

The six parameters were chosen as being of interest in designing deicing systems. The maximum collection efficiency and total water catch are critical parameters for evaporative systems. Impingement limits are used extensively for designing the limits of ice protection systems. The 10% impingement limits were included in this parameter list since some use this location to define the limits of ice protection. This assumption may be due to the insensitivity of an airfoil to small amounts of ice or based on user assumptions of the software's accuracy. The six parameters were measured for the experimental data and for each of the predicted runs. The values were then compared by absolute value, percent difference and for impingement limits by percent chord difference. Results will be shown for the average comparisons as well as a statistical analysis of the software accuracy.

A. LEWICE Comparisons

Comparisons of the six parameters were made between LEWICE and the experimental data. LEWICE was run five times for each condition in the database. In the first option, LEWICE was run in default mode using the embedded potential flow solver and ignoring effects due to splashing and breakup. This option is labeled "PF-NS" (potential flow, no splashing) in some charts. Since the splashing and breakup model is not complete, it can be activated or deactivated by the user. In the second option, LEWICE was run using the potential flow solver and considering splashing. This option is labeled "PF-S". Although all effects are modeled, this report will refer to the splashing, breakup and bouncing model as simply the splashing model since droplet splashing had a much larger effect on the results than droplet breakup. In the third option, the Naviér-Stokes flow solver WIND replaced the potential flow solver. Grids for the Naviér-Stokes solver were created using the ICEG2D grid generator. Default options were used in ICEG2D to control grid density. While a detailed grid resolution study was not performed, certain grids were evaluated by increasing the grid density. It was determined that the default grid resolution was sufficient for these cases. The third option did not include the splashing model and was labeled "NS-NS" (Naviér-Stokes, no splashing). In the fourth option, splashing were considered along with using the Naviér-Stokes flow solver. This option is labeled "NS-S".

A final set of comparisons was performed using LEWICE with the potential flow option and ignoring splashing but made two other adjustments to assess their effect. First, the angle of attack input to LEWICE was altered such that the pressure coefficient distribution produced by the potential flow solver matched pressure tap data from the experiment. This alteration is similar to the angle of attack adjustments made in the previous report on ice shape validation. Second, a 27-bin drop size distribution was used to more accurately model the impinging water. 27 bins were chosen since this matched the total number of "bins" from the FSSP and OAP instrumentation and thus required no interpolation of the drop size distribution. This second variation required modification to LEWICE since the release versions could only run 10-bin distributions. This set of comparisons was chosen to consider the effect of other variables on the accuracy of the solution. Of these two adjustments, the utilization of a 27-bin drop size distribution had by far the larger effect on collection efficiency. In this report, the author will refer to this set of calculations as the "27-bin" or "LEWICE-adj." results. In the reports on the experimental data[9-11], experimental results are compared to "LEWICE". Those results refer to the "LEWICE-adj." results described in this paper. For the maximum collection efficiency parameter, a sixth comparison was included. This last comparison shows the difference between the experimental data and the analytical prediction provided by the scaling equations[40].

1. Maximum Collection Efficiency

The maximum collection efficiency (β_{max}) is simply the highest water collection efficiency value. Only the magnitude of this value was compared. No effort was made to quantitatively compare the location of maximum collection efficiency from experiment with the corresponding location in LEWICE. Qualitatively, the peak values seemed to match very well. Values for all the parameters were extracted from the curves and translated to an Excel spreadsheet for comparison. For β_{max}, comparisons were also made to the values predicted from the scaling equations[40]. Figure 15 shows the results of the statistical comparison.

Figure 15: Comparison of Maximum Collection Efficiency

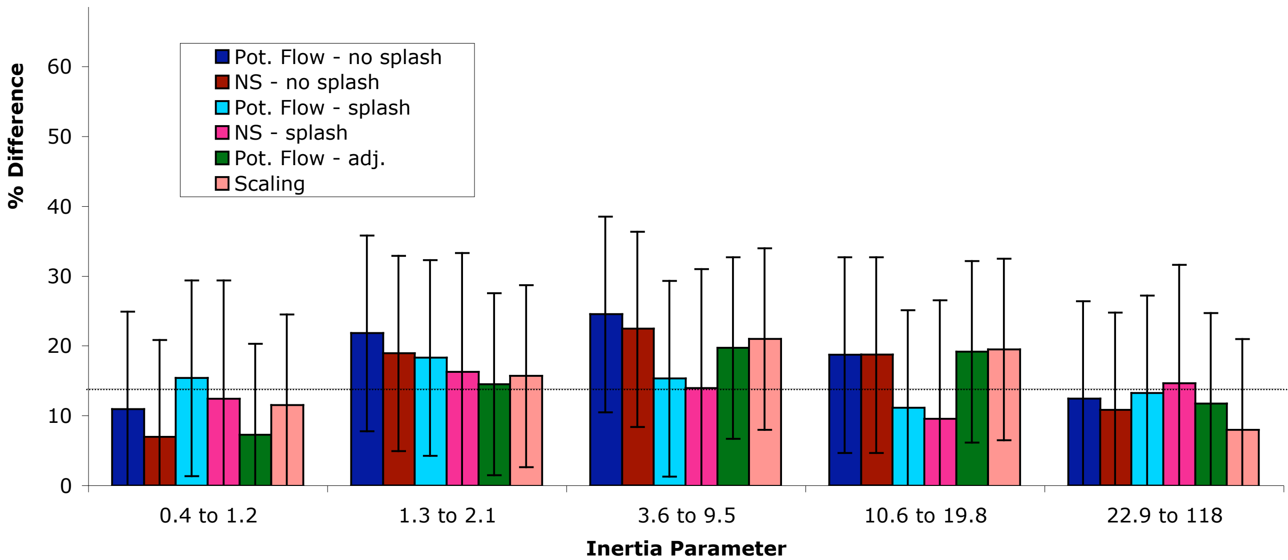

This figure shows the variation as a function of inertia parameter where the inertia parameter is given by

$$K_o = 0.125 + \left(\frac{\rho_w d^2 V}{18 \mu_w D} - 0.125 \right) \left(\frac{1}{0.8388 + 0.001483 \mathrm{Re} + 0.1847 \sqrt{\mathrm{Re}}} \right)$$

Drop size in this equation refers to the MVD value. The first two inertia parameter data groups (0.4 to 1.2 and 1.3 to 2.1) represent Appendix C conditions while the last three groupings indicate conditions where the MVD was in the SLD regime. The five data groupings were chosen such that each group contained approximately the same number of data points while preserving natural divisions within the data. For example, no data was collected in the inertia parameter range of 2.2 to 3.5. The solid bars in this chart represent the average difference between the prediction and the experimental data. The vertical error bars denote one standard deviation from the average and show the variability of the predictions. The dashed horizontal line shows an estimate of the experimental error. This error is only an estimate and refers to the overall confidence of the data. No measure of the error of individual parameters was possible[39].

While there is some scatter in the comparisons, almost all of the results show accuracy within 30% of the experimental data. The average comparisons vary from a low of 6% to 22%. Replacing the potential flow solver with Naviér-Stokes resulted in an improvement in each range, although the average improvement was only 3%. Including the splashing effects improved the results for each range except for the smallest and largest drop sizes. In the low range, splashing effects decreased the accuracy by 6%. This indicates that the splashing threshold was set too low in the empirical model. The effect at the highest inertia parameter may indicate that the re-impingement is not accurately modeled. The two inertia ranges from 3.6 to 9.5 and 10.6 to 19.8 include the other SLD inertia ranges. In this range, the splashing model improves the accuracy of β_{max} by up to 10%, a factor of two (20% to 10%). The adjustments for drop size distribution and flow angle had the greatest effect at the lower inertia range and increased accuracy up to 5%. Comparisons at the approximate average variation from the experiment are shown in Figure 16 for the Appendix C range and in Figure 17 for the SLD range. The data for these plots were taken from the Twin Otter Tail Condition at 4° AOA for the 21 and 79 micron cases respectively. As this case shows, it was not unusual for the splashing model to over compensate at the leading edge and remove more mass than the experiment might indicate.

Figure 16: Average "Appendix C" Comparison for β_{max}

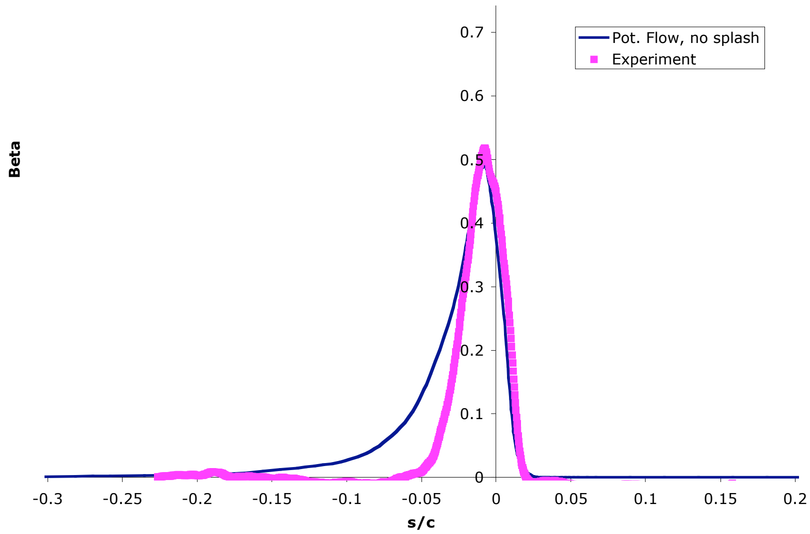

Figure 17: Average SLD Comparison

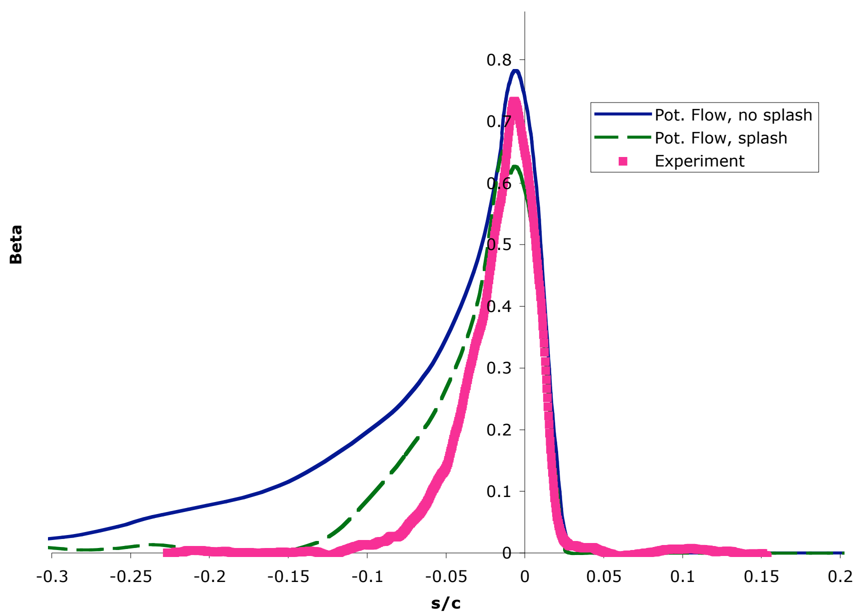

The figure above shows a potentially negative effect of using a model for splashing. While the overall shape of the curve has been improved by using the model, the prediction of β_{max} became worse and resulted in an under prediction for this case. For design purposes, it is preferable to have a conservative estimate. Over prediction is less frequently seen when using the splashing model. This is shown in Figure 18 below. Non-splashing cases over predict water catch and maximum collection efficiency in 75% of the conditions and the amount of under prediction is usually slight. While the splashing model is more accurate overall, it resulted in a reversal of the cases over predicted. A significant majority of cases now under predict water mass flux and β_{max} when using the splashing model. Some adjustments may be needed to the model to compensate for this effect.

Figure 18: Percentage of Cases Over Predicted

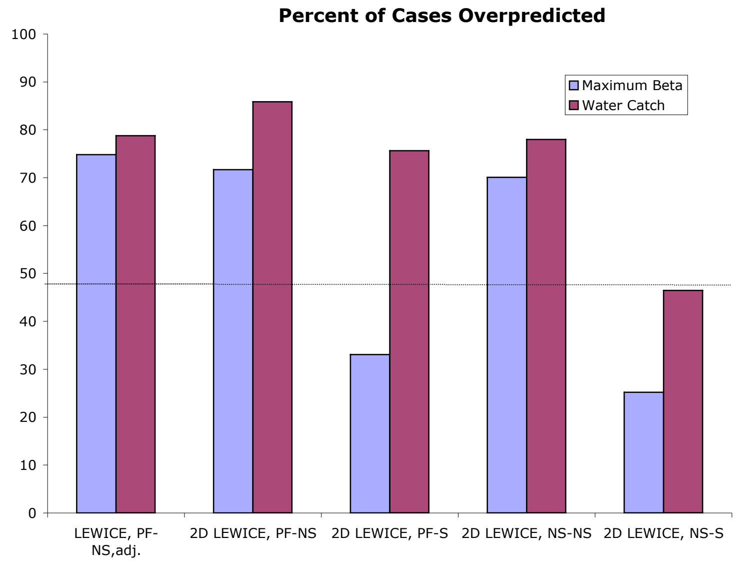

The effect of re-impingement can be seen by the excellent prediction of the scaling parameter in the highest inertia parameter range. The scaling parameter does not include splashing yet showed a better prediction than LEWICE in this range. This indicates that re-impingement of splashed mass occurs in this regime. The scaling methodology outperformed LEWICE without the splashing model but overall was less accurate once the splashing model was included. The accuracy of the scaling equations decreased for thin airfoils and at 8° AOA since they were derived from cylinder data. Similar trends were not evident in the LEWICE results. Figure 19 shows the scaling curve as a function of inertia parameter. This figure contains a fair amount of scatter, yet it seems clear that for K_o values of 20 or more, there are several cases where the measured β_{max} shows a value very close to the analytical prediction that ignores splashing. This is a strong indication that re-impingement becomes important at high inertia parameter values.

Figure 19: Effect of Inertia Parameter on β_{max}

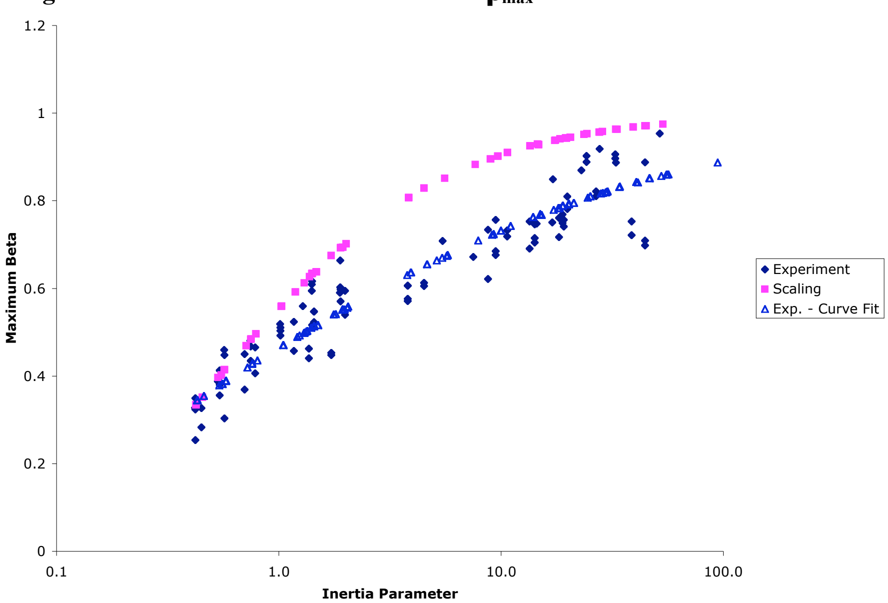

The curve fit in this figure was obtained using the following equation: $\beta_o = \frac{a(K_o - 0.125)^n}{1 + a(K_o - 0.125)^n}$ where a = 0.94 and n = 0.4765 versus a = 1.4 and n = 0.84 from the scaling equations. The curve fit has a regression coefficient (R^2) of 0.84.

2. Total Mass Flux

The total mass flux was obtained by integrating the collection efficiency values with respect to the wrap distance, $\dot{m} = \frac{LWC * V}{c} * \int \beta ds$. Percentage differences were calculated and tabulated with the other results. Statistical averages were also measured for this variable. Figure 20 shows the prediction of mass flux for the five LEWICE scenarios. The scaling equations do not provide a prediction of mass flux. Once again, the solid bars show the average difference between the prediction and experiment while the vertical error bars show the variability (standard deviation) of the results.

Figure 20: Comparison of Total Mass Flux

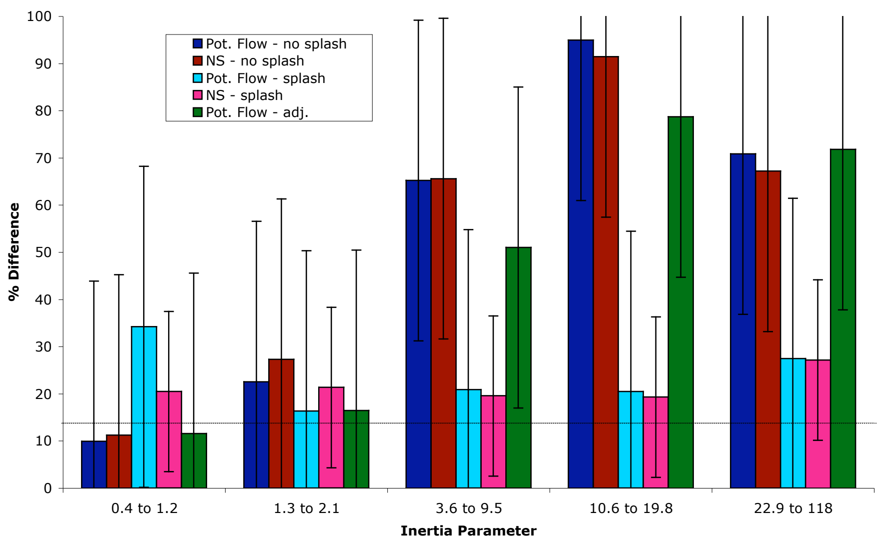

This figure best demonstrates the improvement achieved by using the splashing model. Changing the flow solver to Naviér-Stokes had very little effect on water catch and while using a 27-bin drop size distribution improved the results 15% for the SLD cases, there is a significant over prediction of water catch if splashing is not included. The splashing model removes too much mass in the lowest drop size range, but the improvement in the SLD range is close to 50%. This represents a three to four-fold improvement in accuracy for water mass flux (from a difference of 60% or 80% to a 20% difference). The average difference in the SLD range is now comparable to the accuracy for the Appendix C cases. However, the increased accuracy is somewhat countered by the increase in the number of cases that under predict mass. This can be seen in Figure 21 that shows a comparison for a case near the statistical average. The case chosen was the 168 MVD case for the Twin Otter tail with a 45-min. ice shape attached. In this condition, the overall mass flux was improved because the long "tails" of the impingement limits were splashed away. However, both the experiment and the non-splashing results show a significant impingement on the lower horn of the ice shape that is being removed by the splashing model. This under prediction has significant repercussions for ice accretion cases in SLD and for cases that combine the splashing model with boot operation. This result indicates that either splashing is less vigorous than predicted by the model or that re-impingement is greater than predicted, or both.

Figure 21: Average Case for Total Water Mass Flux

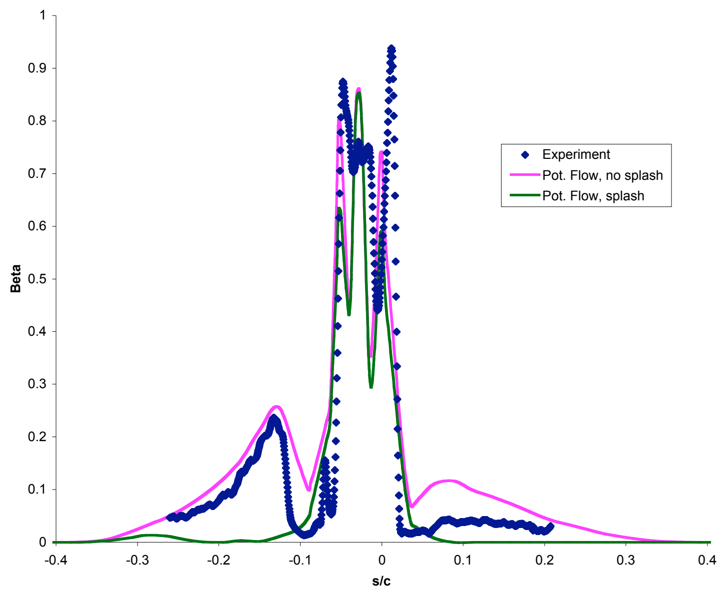

3. *Impingement Limits*

The impingement limits for the upper and lower surface were defined as the x/c location from the leading edge where the collection efficiency last reached 1%. For the ice shape cases, x/c=0 represents the leading edge of the clean airfoil, not the ice shape. Due to small variations in the experimental data, a definition of zero collection efficiency could not be used. This variation is probably due to the difficulty in translating reflectance data to collection efficiency. A computer program was written to extract impingement values from both the experimental data files and from the LEWICE predictions. The values extracted by the software for the experimental data compared well with experimental impingement limit results tabulated in the experimental data report[11]. There were still errors in data collection using this process. Several SLD cases in the experimental database clearly indicate that impingement continued past the limits where blotter strips were installed. In this case, the comparison may show an erroneous result since LEWICE will predict the impingement that the blotter strip technique could not measure. It is believed that the overall comparisons are still valid despite these limitations. The 10% limits followed the same procedure for comparison and were much more clearly defined in both the experimental data and the predicted values.

Figures 22 and 23 show the statistical comparison between LEWICE and the experimental data for the lower and upper 1% impingement limits, respectively. There is less variation in the impingement limit results for the various scenarios. Both the average value (solid bars) and the standard deviation (error bars) show a smaller variation. On average, there was approximately a 4% chord improvement to the lower impingement limit predictions when using the splashing model and only a 2% improvement to the upper limit predictions. Appendix C cases were well predicted whether or not the splashing model was used. Use of a 27-bin drop size distribution or use of a Naviér-Stokes solver did not add significantly to the accuracy of the impingement limits.

The variation from experiment increased for the splashing model in the largest inertia parameter range. In this respect, the experimental data results strongly suggest that re-impingement of water is greater in this regime than the amount predicted by the LEWICE splashing model. It is hypothesized since splashed drop sizes are proportional to the impact drop sizes that for impact drop sizes in the 50 µm to 100 µm range, the splashed drop sizes are so small that they are entrained in the air stream while for larger impact drop sizes much of the splashed mass may re-impinge due to the larger splashed drop sizes. Figure 14, which was used to illustrate the collection efficiency parameters, is also an example of an average comparison for impingement limits. The case used for that illustration was from the MS-317 airfoil at 0° AOA and a 92 µm MVD. The increased accuracy of the splashing model does result in a larger number of cases in which an undesirable under prediction can occur. Figure 24 shows the average over prediction for the impingement limit prediction. This figure shows that without splashing. 60% to 80% of cases result in an over prediction of the impingement limit. When splashing is included, the lower limit is still over predicted in 60% of the cases (40% under predicted) while the upper impingement limit is under predicted 80% of the time when using potential flow and 85% of the time when using a Naviér-Stokes solver. Figure 20 showed an example where under prediction of the impingement limit would be an undesirable result.

Figure 22: Comparison of Lower Impingement Limit

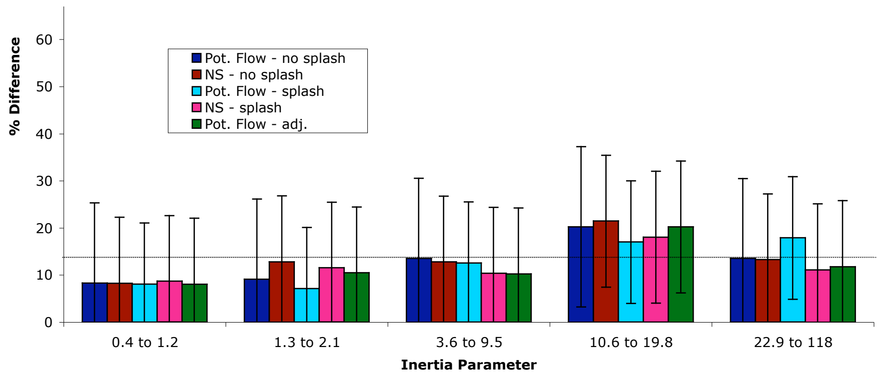

Figure 23: Comparison of Upper Impingement Limit

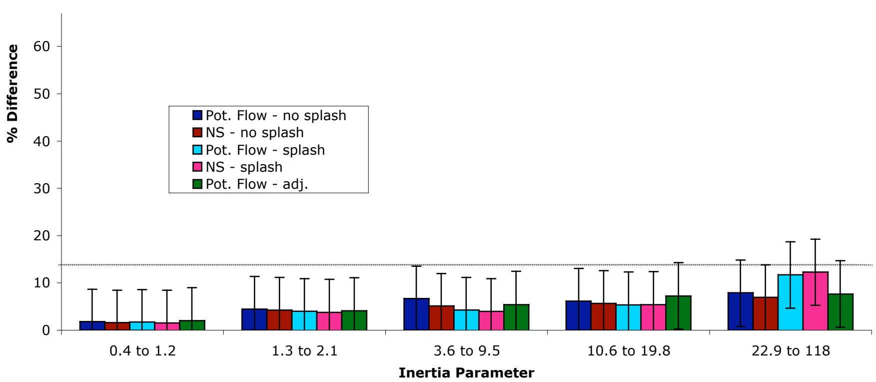

Figure 24: Percent Over Prediction for Impingement Limit

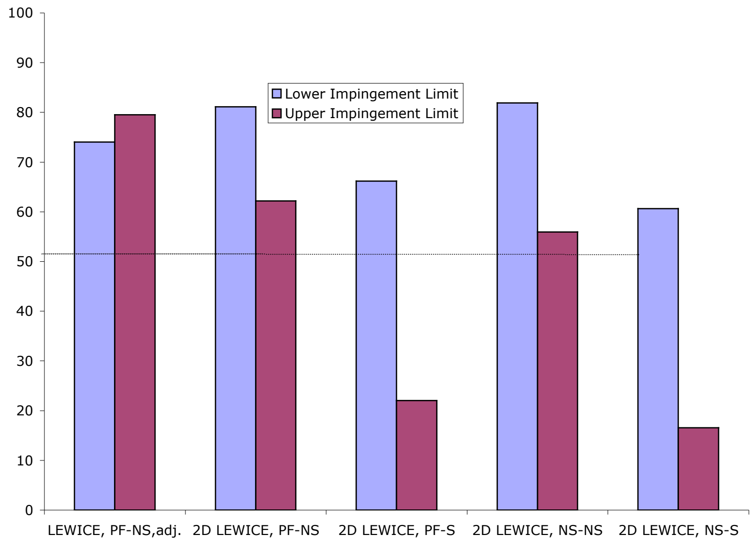

4. 10% Impingement Limits

The upper and lower 10% limits were defined in the same manner as the impingement limits in the previous section. In this case, a collection efficiency value of 10% ($\beta = 0.1$) was used to define the limit. Several users of the LEWICE software have used the $\beta = 0.1$ limit because they either are not concerned with small levels of residual ice or because they do not trust the accuracy of the software. The statistical comparisons of the last two parameters are shown in Figs. 25 and 26 for the upper and lower 10% limit, respectively. These parameters have the highest accuracy of all of the parameters presented. The predictions for the Appendix C cases are extremely accurate. The variability (standard deviation, shown by the error bars) is very low for this parameter, Once again, the addition of a Naviér-Stokes flow solution or the inclusion of additional drop sizes in the distribution did not greatly alter the accuracy of the prediction. The addition of the splashing model showed a small improvement to the upper 10% limit and a significant improvement to the lower 10% limit. For SLD conditions, the average improvement (shown by the difference in the solid bars) was 11%, reducing the discrepancy from an average difference of 14% chord without the splashing model to an average difference of 3% chord (a four-fold increase in accuracy) when the model is used. The MS-317 case showed in Fig. 14 is also representative of the average accuracy of LEWICE for the 10% impingement limits. Figure 27 shows the percentage of cases over predicted for these two parameters. This figure shows that while the accuracy of the lower 10% impingement limit was greatly improved by using the splashing model, the percentage over predicted remained approximately 70%. The upper 10% limit changed from slightly over 50% over predicted when splashing was not considered to 40% over predicted for potential flow and 20% over predicted when using Naviér-Stokes. However, given the overall accuracy of the 10% limits, this may not be a concern.

Figure 25: Comparison of Upper 10% Limit

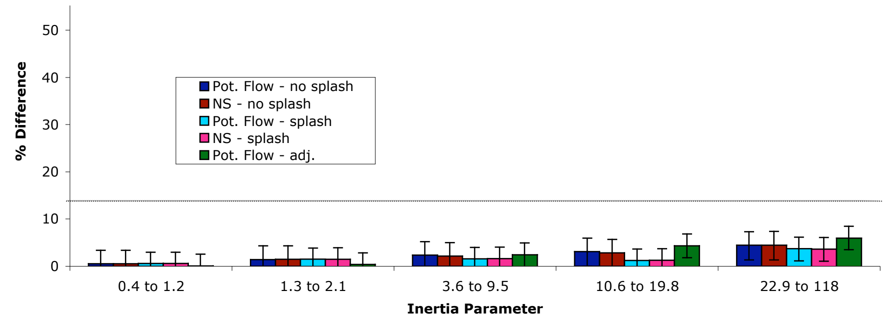

Figure 26: Comparison of Lower 10% Limit

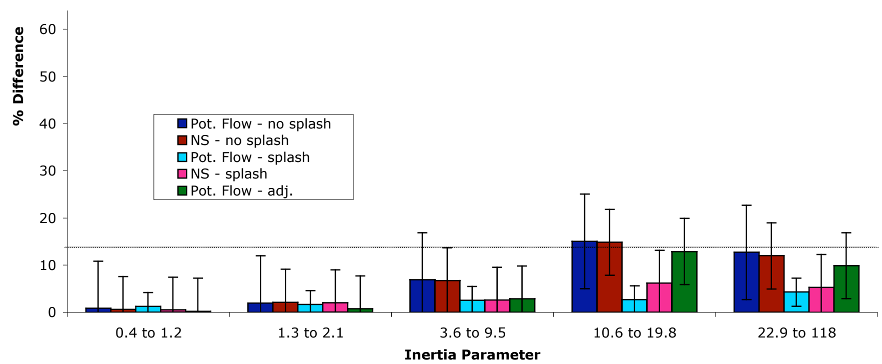

Figure 27: Percentage Over Predicted for 10% Impingement Limit

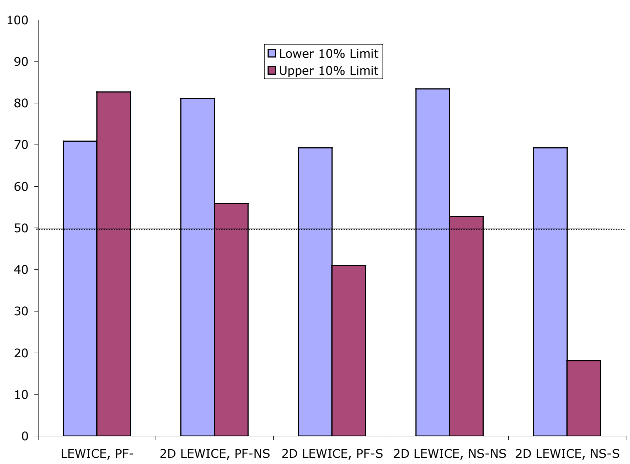

VIII. Conclusions

A review of the physical effects of large droplet phenomena confirmed that droplet splashing is the primary physics that is not modeled in icing software in this drop size regime. Several other phenomena such as drop breakup, drop-drop interactions and changes in drag and lift were also covered. Empirical models for these phenomena were presented. The resulting effects of the additional physics on water collection in LEWICE were presented.

The results show that the empirical splashing models in the open literature could only account for splashing effects near the leading edge. The models, all of which are based on the velocity component normal to the surface, could not explain the measured decrease in water collection near the impingement limits. However, it was necessary to extrapolate values from that empirical data for this effort. It is hypothesized that droplets that impact at high total velocities (> 30 m/s) but low impact angles (< 20°) may rebound in a manner different than the current experimental data at the lower velocities. A new model based on physical arguments was proposed to account for the additional physical phenomena that occur in the SLD regime.

The accuracy of the model was tested against a voluminous database of collection efficiencies that had been accumulated in the IRT over the last twenty years. A comprehensive comparison was performed that compared maximum collection efficiency, total water mass flux, upper & lower impingement limits, and upper & lower 10% limits. Comparisons were made with and without the new model to demonstrate its effectiveness. Comparisons were also made to assess the effect of using a Naviér-Stokes flow solver and to assess the effect of other adjustments including the use of 27-bin drop size distributions instead of 10-bin distributions.

The comparisons showed that the inclusion of a splashing model improved the prediction of all six parameters for the SLD range. For SLD conditions, the accuracy of maximum collection efficiency doubled for some inertia parameter ranges. The accuracy increased by a factor of four for water mass flux and the lower 10% impingement limit. Other parameters showed improvement in the SLD range as well. Use of a Naviér-Stokes flow solution did not greatly enhance the accuracy of the prediction. Use of a 27-bin drop size distribution increased accuracy slightly.

The analysis showed that the model can cause adverse effects for Appendix C cases and may increase the likelihood of under prediction of the six parameters for Appendix C or SLD conditions. The model also seems to under estimate the effect of re-impingement of splashed mass for the largest impinging drop sizes. The formulation of the empirical model suggests that velocity is at least as important of a variable as drop size for splashing and breakup. Since the model is empirical in nature, care should be exercised in using the splashing model beyond the air speed used in the experiments (175 mph).

X. References

1. "In-flight Icing Encounter and Loss of Control Simmons Airlines, d.b.a. American Eagle Flight 4184 Avions de Transport Regional (ATR) Model 72-212, N401AM, Roselawn, Indiana October 31, 1994", NTSB Report Number: AAR-96-01.

2. G. A. Isaac, S. G. Cober, J. W. Strapp, D. Hudak, T. P. Ratvasky, D. L. Marcotte, and F. Fabry, "Preliminary Results from the Alliance Research Study (AIRS)", AIAA-2001-393, Jan. 2001.

3. M. Potapczuk, "Ice Mass Measurements: Implications for the Ice Accretion Process", AIAA-2003-387, Jan. 2003.

4. T. Bond, M. Potapczuk and D. Miller, " Overview of SLD Engineering Tool Development," AIAA-2003-386, Jan. 2003.

5. Gent, J. Ford and R. Moser, D. Miller, "Results from SLD Mass Loss Tests in the ACT Luton Icing Research Wind Tunnel," AIAA-2003-389, Jan. 6-9, 2003.

6. Tan, S. C. and Papadakis, M., " General Effects of Large Droplet Dynamics on Ice Accretion Modeling," AIAA 2003-392, Jan. 2003.

7. Rutkowski, A., Wright, W. B. and Potapczuk, M. G., "Numerical Study of Droplet Splashing and Re-Impingement," AIAA 2003-388, Jan. 2003.

8. W. Wright, M. Potapczuk, "Empirical Modeling of SLD Physics", AIAA-2004-412, Jan. 2004.

9. Papadakis, M., Elangonan, R., Freund, Jr., G. A., Breer, M., Zumwalt, G. W. and Whitmer, L., "An Experimental Method for Measuring Water Droplet Impingement Efficiency on Two- and Three-Dimensional Bodies," NASA CR 4257, Nov. 1989.

10. Papadakis, M., Breer, M., Craig, N. and Liu, X., "Experimental Water Droplet Impingement Data on Airfoils, Simulated Ice Shapes, an Engine Inlet and a Finite Wing," NASA CR 4636, DOT/FAA/CT-TN93/18, Dec. 1994.

11. Papadakis, M., Hung, K. E., Vu, G .T., Yeong, H. W., Bidwell, C. S., Breer, M. D., Bencic, T. J., "Experimental Investigation of Water Droplet Impingement on Airfoils, Finite Wings, and an S-Duct Engine Inlet, NASA TM 2002-211700, Oct. 2002.

12. Wright, W. B. and Rutkowski, A., “Validation Results for LEWICE 2.0,” NASA CR 208690, Nov. 1998.

13. Bush, R. H. , Power, G. D. and Towne, C. E., “WIND: The Production Flow Solver of the NPARC Alliance,” AIAA 98-0935, Jan. 1998.

14. Wright, W. B., "Users Manual for the NASA Glenn Ice Accretion Code LEWICE Version 3.0," available on the NASA LEWICE 3.0 release CD, Apr. 2003.

15. Thompson, D. S. and Soni, B. K., “ICEG2D: A Software Package for Ice Accretion Prediction,” AIAA 2003-1070, Jan. 2003

16. Clift, R., Grace, J. R., and Weber, M. E., “Bubbles, Drops, and Particles,” Academic Press, New York, 1978.

17. Tavlarides, L. T., Coulalogou, C. A., Zeitlin, M. A., Klinzing, G. E., Gal-or, B., "Bubble and Drop Phenomena," Ind. And Eng. Chem. V. 62, no. 11, pp. 6-27, Nov. 1970.

18. Michaelides, E. E., "Review – The Transient Equation of Motion for Particles, Bubbles, and Droplets," J. Fluids Engr., v. 119, pp. 233-246, June 1997.

19. Krzeczkowski, S. A., "Measurement of Liquid Droplet Disintegration Mechanism," int. J. Multiphase Flow, v. 6, pp. 227-239, 1980.

20. Hsiang, L. P. and Faeth. G. M., "Secondary Drop Breakup in the Deformation Regime," AIAA 92-0110, Jan. 1992.

21. Ibrahim, E. A., Yang, H. Q., and Przekwas, A. J., "Modeling of Spray Droplets Deformation and Breakup," J. Prop., v. 9, No. 4, pp. 651-654, 1993.

22. Dai, Z. and Faeth, G. M., "Temporal Properties of Multimode Secondary Droplet Breakup," AIAA 99-0333, Jan. 1999.

23. Stow, C. D., and Hadfield, M. G., "An Experimental Investigation of Fluid Flow Resulting from the Impact of a Water Drop with an Unyielding Dry Surface," Proc. R. soc. Lond. A v. 373, pp. 419-441, 1981.

24. Macklin, W. C. and Metaxas, G. J., "Splashing of Drops on Liquid Layers," J. App. Phys., v. 47, No. 9, pp. 3963-3970, Sept. 1976.

25. Jayarante, O. W. and Mason, B. J., "The Coalescence and Bouncing of Water Drops at an Air/Water Interface," proc. Roy. Sci. A., v. 280, pp. 545-565, 1965.

26. Wright, A. C., "A Physically-Based Model of the Dispersion of Splash Droplets Ejected from a Water Drop Impact," Earth Surf. Proc. And Landforms, v. 11, pp. 351-367, 1986.

27. Harlow F. H. and Shannon, J, P., "The Splash of a Liquid Drop," J. App. Phys., v. 38, No. 10, pp. 3855-3866, 1967.

28. Yarin. A. L. and Weiss, D. A., "Impact of Drops on Solid Surfaces: Self-Similar Capillary Waves, and Splashing as a New Type of Kinematic Discontinuity," J. Fluid Mech., v. 283, pp. 141-173, 1995.

29. Weiss D. A., "Periodischer Aufprall monodisperser Tropen gleicher Geschwindigkeit auf feste Oberflächen," Mitteilungeen aus dem Max-Plank-Institut für Stromungsforschung, Gottingen, Nr. 112, 1993.

30. Rein, M., "Phenomena of Liquid Drop Impact on Solid and Liquid Surfaces," Fl. Dyn. Res., v. 12, pp. 61-93, 1993.

31. Chandra, S. and Avedisian, C. T., "On the Collision of a Droplet with a Solid Surface," Proc. Roy. Soc. Lond. A, v. 432, pp. 13-41, 1991.

32. Hirt, C. W., Nicholls, B. D., "Volume of Fluid Method for Dynamic Free Boundary," J. Comp. Phys., v.39, 1981.

33. Trapaga, G. and Szekely, J., "Mathematical Modeling of the Isothermal Impingement of Liquid Drops in the Spraying Process," Metallurgical Transactions B, v. 22B, pp. 901-914, Dec. 1991.

34. Mundo, C., Sommerfeld, M., and Tropea, C., “Droplet-Wall Collisions: Experimental Studies of the Deformation and Breakup Process,” Int. J. Multiphase Flow, v. 21, No. 2, pp. 151-173, 1995.

35. Mundo, C., Tropea, C. and Sommerfeld, M., “Numerical and Experimental Investigation of Spray Characteristics in the Vicinity of a Rigid Wall,” Exp. Thermal and Fl. Sci., v. 15, pp. 228-237, 1997.

36. Mundo, C., Sommerfeld, M., and Tropea, C., “On the Modeling of Liquid Sprays Impinging on Surfaces,” Atomization and Sprays, v. 8, pp. 625-652, 1998.

37. Feo, A., Personal Communication, Dec. 2003.

38. Trujillo, M. F., Matthews, W.S., Lee, C.F., and Peters, J.E., "Modeling and Experiment of Impingement and Atomization of a Liquid Spray on a Wall," Int. J. Engine Research, v. 1, No. 1, pp. 87-104, 2000.

39. Papadakis, M., Personal Communication, Apr. 2004.

40. D. Anderson and J. Tsao, " Additional Results of Ice-Accretion Scaling at SLD Conditions," AIAA-2003-390, Jan. 6-9, 2003

REPORT DOCUMENTATION PAGE	*Form Approved* *OMB No. 0704-0188*

1. AGENCY USE ONLY (*Leave blank*)	2. REPORT DATE	3. REPORT TYPE AND DATES COVERED
	March 2005	Final Contractor Report

4. TITLE AND SUBTITLE

Validation Results for LEWICE 3.0

5. FUNDING NUMBERS

WBS–22–728–41–10
NAG3–00145

6. AUTHOR(S)

William B. Wright

7. PERFORMING ORGANIZATION NAME(S) AND ADDRESS(ES)

QSS Group, Inc.
21000 Brookpark Road
Cleveland, Ohio 44135

8. PERFORMING ORGANIZATION REPORT NUMBER

E–15007

9. SPONSORING/MONITORING AGENCY NAME(S) AND ADDRESS(ES)

National Aeronautics and Space Administration
Washington, DC 20546–0001

10. SPONSORING/MONITORING AGENCY REPORT NUMBER

NASA CR—2005-213561
AIAA–2005–1243

11. SUPPLEMENTARY NOTES

Prepared for the 43rd Aerospace Sciences Meeting and Exhibit sponsored by the American Institute of Aeronautics and Astronautics, Reno, Nevada, January 10–13, 2005. Project Manager, Thomas Bond, Turbomachinery and Propulsion Systems Division, NASA Glenn Research Center, organization code RTI, 216–433–3900.

12a. DISTRIBUTION/AVAILABILITY STATEMENT

Unclassified - Unlimited
Subject Category: 02

Available electronically at http://gltrs.grc.nasa.gov/GLTRS
This publication is available from the NASA Center for AeroSpace Information, 301–621–0390.

12b. DISTRIBUTION CODE

13. ABSTRACT ***(Maximum 200 words)***

A research project is underway at NASA Glenn to produce computer software that can accurately predict ice growth under any meteorological conditions for any aircraft surface. This report will present results from version 3.0 of this software, which is called LEWICE. This version differs from previous releases in that it incorporates additional thermal analysis capabilities, a pneumatic boot model, interfaces to computational fluid dynamics (CFD) flow solvers and has an empirical model for the supercooled large droplet (SLD) regime. An extensive comparison of the results in a quantifiable manner against the database of ice shapes and collection efficiency that have been generated in the NASA Glenn Icing Research Tunnel (IRT) has also been performed. The complete set of data used for this comparison will eventually be available in a contractor report. This paper will show the differences in collection efficiency between LEWICE 3.0 and experimental data. Due to the large amount of validation data available, a separate report is planned for ice shape comparison. This report will first describe the LEWICE 3.0 model for water collection. A semi-empirical approach was used to incorporate first order physical effects of large droplet phenomena into icing software. Comparisons are then made to every single element two-dimensional case in the water collection database. Each condition was run using the following five assumptions: 1) potential flow, no splashing; 2) potential flow, no splashing with 21 bin drop size distributions and a lift correction (angle of attack adjustment); 3) potential flow, with splashing; 4) Navier-Stokes, no splashing; and 5) Navier-Stokes, with splashing. Quantitative comparisons are shown for impingement limit, maximum water catch, and total collection efficiency. The results show that the predicted results are within the accuracy limits of the experimental data for the majority of cases.

14. SUBJECT TERMS

Aircraft icing; Ice formation

15. NUMBER OF PAGES

32

16. PRICE CODE

17. SECURITY CLASSIFICATION OF REPORT	18. SECURITY CLASSIFICATION OF THIS PAGE	19. SECURITY CLASSIFICATION OF ABSTRACT	20. LIMITATION OF ABSTRACT
Unclassified	Unclassified	Unclassified	